Intrinsic radiomic expression patterns after 20 Gy demonstrate early metabolic response of oropharyngeal cancers

Kyle J. Lafata[a)]
Department of Radiation Oncology, Duke University School of Medicine, Durham, NC, USA
Department of Radiology, Duke University School of Medicine, Durham, NC, USA
Department of Electrical & Computer Engineering, Duke University Pratt School of Engineering, Durham, NC, USA
Medical Physics Graduate Program, Duke University, Durham, NC, USA

Yushi Chang and Chunhao Wang
Department of Radiation Oncology, Duke University School of Medicine, Durham, NC, USA
Medical Physics Graduate Program, Duke University, Durham, NC, USA

Yvonne M. Mowery
Department of Radiation Oncology, Duke University School of Medicine, Durham, NC, USA
Department of Head and Neck Surgery & Communication Sciences, Duke University School of Medicine, Durham, NC, USA

Irina Vergalasova
Department of Radiation Oncology, Rutgers Cancer Institute of New Jersey, Robert Wood Johnson Medical School, New Brunswick, NJ, USA

Donna Niedzwiecki
Department of Biostatistics and Bioinformatics, Duke University School of Medicine, Durham, NC, USA

David S. Yoo
Department of Radiation Oncology, Duke University School of Medicine, Durham, NC, USA

Jian-Guo Liu
Department of Mathematics, Duke University, Durham, NC, USA
Department of Physics, Duke University, Durham, NC, USA

David M. Brizel
Department of Radiation Oncology, Duke University School of Medicine, Durham, NC, USA
Department of Head and Neck Surgery & Communication Sciences, Duke University School of Medicine, Durham, NC, USA

Fang-Fang Yin
Department of Radiation Oncology, Duke University School of Medicine, Durham, NC, USA
Medical Physics Graduate Program, Duke University, Durham, NC, USA

(Received 26 January 2021; revised 26 March 2021; accepted for publication 25 April 2021; published 2 June 2021)

Purpose: This study investigated the prognostic potential of intra-treatment PET radiomics data in patients undergoing definitive (chemo) radiation therapy for oropharyngeal cancer (OPC) on a prospective clinical trial. We hypothesized that the radiomic expression of OPC tumors after 20 Gy is associated with recurrence-free survival (RFS).

Materials and Methods: Sixty-four patients undergoing definitive (chemo)radiation for OPC were prospectively enrolled on an IRB-approved study. Investigational ^{18}F-FDG-PET/CT images were acquired prior to treatment and 2 weeks (20 Gy) into a seven-week course of therapy. Fifty-five quantitative radiomic features were extracted from the primary tumor as potential biomarkers of early metabolic response. An unsupervised data clustering algorithm was used to partition patients into clusters based only on their radiomic expression. Clustering results were naïvely compared to residual disease and/or subsequent recurrence and used to derive Kaplan-Meier estimators of RFS. To test whether radiomic expression provides prognostic value beyond conventional clinical features associated with head and neck cancer, multivariable Cox proportional hazards modeling was used to adjust radiomic clusters for T and N stage, HPV status, and change in tumor volume.

Results: While pre-treatment radiomics were not prognostic, intra-treatment radiomic expression was intrinsically associated with both residual/recurrent disease ($P = 0.0256$, χ^2 test) and RFS (HR = 7.53, 95% CI = 2.54–22.3; $P = 0.0201$). On univariate Cox analysis, radiomic cluster was associated with RFS (unadjusted HR = 2.70; 95% CI = 1.26–5.76; $P = 0.0104$) and maintained significance after adjustment for T, N staging, HPV status, and change in tumor volume after 20 Gy (adjusted HR = 2.69; 95% CI = 1.03–7.04; $P = 0.0442$). The particular radiomic characteristics associated with outcomes suggest that metabolic spatial heterogeneity after 20 Gy portends complete and durable therapeutic response. This finding is independent of baseline metabolic imaging

characteristics and clinical features of head and neck cancer, thus providing prognostic advantages over existing approaches.

Conclusions: Our data illustrate the prognostic value of intra-treatment metabolic image interrogation, which may potentially guide adaptive therapy strategies for OPC patients and serve as a blueprint for other disease sites. The quality of our study was strengthened by its prospective image acquisition protocol, homogenous patient cohort, relatively long patient follow-up times, and unsupervised clustering formalism that is less prone to hyper-parameter tuning and over-fitting compared to supervised learning. [https://doi.org/10.1002/mp.14926]

Key words: imaging biomarker, machine learning, oropharyngeal cancer, radiomics

1. INTRODUCTION

Despite major advances in understanding the pathophysiology of oropharyngeal cancer (OPC) over the past two decades, including the favorable prognosis of human papillomavirus (HPV)-associated disease,[1–5]

the overall treatment approach for this disease has remained relatively unchanged. Standard non-operative management with radiation therapy or chemoradiation remains based on universal prescription doses for all patients, regardless of whether they have HPV-associated or HPV-negative disease. Many strategies are currently being investigated to de-intensify treatment for patients with favorably prognostic disease and intensify therapy for patients with prognostically unfavorable disease. Most of these efforts are based on pre-treatment tumor characteristics. Adaptive therapy represents an alternative approach, in which the treatment program is modified during therapy based on an indication of a favorable or unfavorable response.[6,7] Customized treatment based on individual response represents a precision oncology paradigm with the potential to improve efficacy, while also improving acute and long-term toxicity profiles.[8]

Optimal methods to identify patients for adaptive therapy have not yet been determined, however, and locoregional recurrence is still a major driver for mortality from OPC.[9,10] New diagnostic approaches that accurately capture the appearance, development, and behavior of OPC are critical to guide improved treatment strategies for this unmet clinical need.[11,12] Radiomic sequencing is a promising high-throughput computational technique where medical images are first *transcribed* into mineable data and then *translated* into computational biomarkers. These biomarkers aim to capture the underlying phenotype of a disease, in an effort to predict disease progression and enable personalized therapy. In recent years, pre-treatment radiomic analysis has been applied to head and neck cancer to predict locoregional disease control,[13–18] patient survival,[13,19–21] and radiation-induced normal tissue complications.[22–27]

This paper describes the results of a single-institution, prospective study, where investigational pre- and intra-treatment ^{18}F-fluorodeoxyglucose positron emission tomography (^{18}F-FDG-PET)/computed tomography (CT) acquisition was performed as an imaging biomarker of early therapeutic response. We hypothesized that tumor-specific radiomic expression patterns on PET images acquired after 2 weeks (20 Gy) of definitive (chemo)radiation therapy were intrinsically associated with recurrence free survival (RFS) for patients with OPC. We tested this hypothesis with an investigational intra-treatment PET acquisition protocol and an unsupervised clustering technique to computationally interrogate radiomic patterns of OPC tumors after 20 Gy.

2. MATERIALS AND METHODS

2.A. Overall research design

An overview of our study design is provided in Fig. 1. Additional details pertaining to image acquisition, reconstruction, and processing are provided in Table S1, following the Image Biomarker Standardization Initiative (IBSI) *Reporting Guidelines for Radiomic Studies*.[28,29]

2.B. Patients and treatment

Patients were enrolled onto a single-institution, prospective study (NCT01908504) approved by the institutional review board at Duke University Medical Center. The current research analyzes the subset of patients undergoing curative-intent intensity modulated radiation therapy (IMRT) for biopsy-proven OPC. Patients received definitive IMRT to a total dose of 70 Gy in 35 fractions or 67.5 Gy in 30 fractions. Although chemotherapy was not mandated, most patients received concurrent modified bolus cisplatin (20 mg/m^2 Days 1-5 and Days 29-33), weekly cisplatin, or weekly docetaxel as per standard and long-standing institutional practice. Patients were excluded from subsequent analysis if they (i) had a diagnosis of p16-positive head and neck squamous cell carcinoma of unknown primary; (ii) had prior surgical resection of primary tumor; (iii) presented with multiple synchronous primary tumors; or (iv) received neoadjuvant chemotherapy prior to definitive radiotherapy.

2.C. Patient follow-up and clinical outcomes

Patients were followed every 2-3 months after the completion of therapy with serial physical exam including fiberoptic laryngoscopy, diagnostic PET/CT (3 months after completing radiation therapy) and additional imaging as clinically

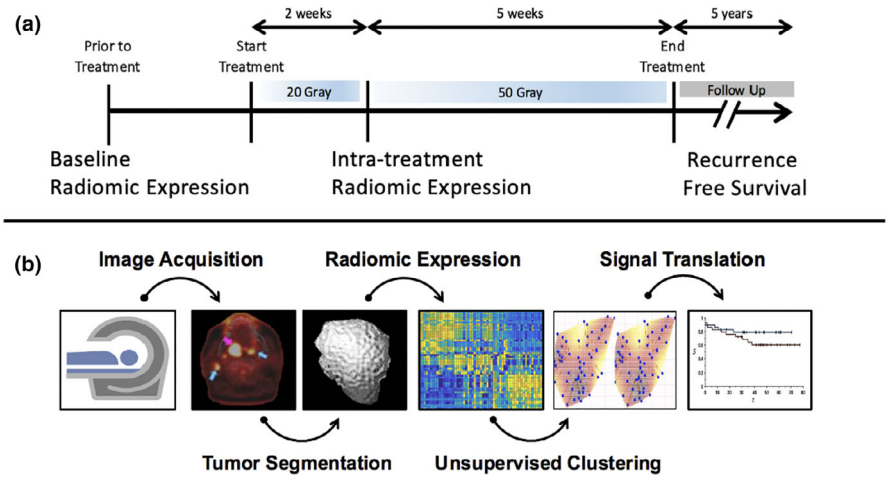

FIG. 1. Overall research design. (a) Prospective clinical trial design to evaluate ^{18}FDG-PET/CT as an intra-treatment imaging biomarker. Patients undergoing definitive radiation therapy (7 weeks, 70 Gy) for oropharyngeal cancer underwent ^{18}FDG-PET/CT prior to treatment and approximately 2 weeks into treatment (2 weeks, 20 Gy) on the same scanner. High-throughput radiomic features were extracted as potential biomarkers of early metabolic response and recurrence free survival data were collected following treatment. (b) Radiomic feature extraction and analysis. The primary tumor gross tumor volume (GTV) was contoured and radiomic features extracted to transcribe the unstructured images into mineable data. Unsupervised data clustering was used to group patients based on intrinsic similarities of their radiomic expression. To test the prognostic value of radiomic expression, the clustering solutions were naïvely compared to recurrence-free survival. [Color figure can be viewed at wileyonlinelibrary.com]

indicated, and biopsy of any lesions suspicious for recurrence. The primary time-to-event clinical endpoint was recurrence-free survival (RFS), defined as the time from RT completion to residual or recurrent disease (local, regional, and/or distant). Patients were censored at the date of last follow-up and median follow-up time was calculated based on the reverse Kaplan-Meier method.

2.D. Image acquisition and reconstruction

As per study protocol, ^{18}F-FDG-PET/CT images were acquired both prior to treatment and 2 weeks into the 7-week course of treatment (i.e., after 20 Gy). All patients were scanned in the Department of Radiation Oncology on the same Siemens Biograph mCT PET/CT imaging system (Siemens Medical Solutions, Knoxville, TN) with a consistent imaging protocol. Total FDG activity was 8-15 mCi depending on patient weight and was administered intravenously after 4 hours of fasting. For each patient, the time-delay from FDG injection to image acquisition (~50-70 minutes) was kept constant from pre-treatment to intra-treatment imaging. PET images were acquired at a standard 54 cm *field-of-view* (400 × 400 matrix size, 2 mm slice thickness) and reconstructed based on an ordered subset expectation maximization (OSEM) algorithm with time-of-flight correction and CT-based attenuation correction. CT images were acquired at an extended 65 cm *field-of-view* (512 × 512 matrix size, 3 mm slice thickness) and reconstructed based on standard filtered back-projection.

2.E. High-throughput radiomic sequencing

To *transcribe* the unstructured PET images into structured, mineable data, we implemented the following high-throughput radiomic feature extraction process. A radiation oncologist manually segmented the gross tumor volume at the primary tumor site (GTVp) on CT, transferred it to PET, visually confirmed the transfer, and made manual adjustments, if necessary. The image was re-sampled to an isotropic resolution of 1.17 mm using a tri-cubic spline interpolation method and the dynamic range was re-binned to 64 gray levels. This fixed bin number approach was adopted based on IBSI recommendations for calibrated intensity units (i.e., SUV) where contrast resolution is considered important.[28] Furthermore, 64 discretized gray levels were chosen based on recommendations to avoid misleading relationships between texture features and SUV.[30]

At time $\tau = \tau_0$, a set of 55 radiomic features (Table S2) were extracted from GTVp on pre-treatment PET images to quantify the baseline metabolic characteristics of each patient's primary tumor. At time $\tau = \tau_{2wk}$, the same radiomic features were extracted from the 2-week PET images to quantify potential early metabolic response to treatment. Thus, given m features and n patients, we define a time-dependent radiomic feature space as the matrix,

$$\mathscr{F}(\tau) = \left(f_{i,j}\right) \in \mathbb{R}^{m \times n} \tag{1}$$

where, the $(i,j)^{th}$ coordinate represents the measured value of the i^{th} radiomic feature as observed on the image of the j^{th} patient at time, τ. By definition, the j^{th} column vector of $\mathscr{F}$,

$$\mathbf{f}_j(\tau) = \left(f_{i,j}\right)_{i=1}^{m} \in \mathbb{R}^m,\ j = 1, 2, \ldots, n, \tag{2}$$

corresponds to the j^{th} patient's radiomic signature, and the i^{th} column vector of $\mathscr{F}^{\dagger}$,

$$\mathbf{f}_i(\tau) = \left(f_{j,i}\right)_{j=1}^{n} \in \mathbb{R}^n,\ i = 1, 2, \ldots, m, \tag{3}$$

corresponds to the i^{th} feature measurement spanning the patient cohort. In general, $\mathbf{f}_j(\tau_0)$ and $\mathbf{f}_j(\tau_{2wk})$ represent shift-invariant radiomic expression patterns derived from pre-

treatment imaging and intra-treatment imaging, respectively, for a given patient.

Each $\mathbf{f}_j(\tau)$ was engineered to collectively capture tumor intensity, fine texture, and coarse texture characteristics on PET. Texture features were averaged over 13 unique directions to approximate a rotationally invariant system. Prior to subsequent analysis, the column vectors in the matrix $\mathscr{F}$ were standardized to zero-mean and unit-variance. Feature extraction was performed in Matlab using custom software previously benchmarked on digital phantoms[31] and tested for compliance with IBSI standards.[28,29] Complete details pertaining to radiomic feature extraction settings are provided in Table S1.

2.F. Unsupervised clustering of radiomic expression patterns

Data clustering (i.e., a type of unsupervised machine learning, where data objects are grouped together based on their intrinsic properties) was used to partition patients into groups based solely on their ^{18}F-FDG-PET radiomic expression patterns prior to and during treatment. The clustering mechanism we chose[32] is motivated by an emerging branch of computational intelligence that explores methodological and structural similarities between quantum systems and learning systems. It assumes that $\mathscr{F}$ is sampled from a canonical ensemble whose probability measure takes the form of a Boltzmann distribution, and thus obeys the following second-order stochastic differential equation,

$$\frac{d^2\mathbf{f}_j}{dt^2} = -\nabla \mathrm{V}(\mathbf{f}_j) - \frac{d\mathbf{f}_j}{dt} + n(t) \tag{4}$$

where, $\mathbf{f}_j$ is an m-dimensional radiomic feature vector defined via Eq. (2), $n(t)$ is a random Gaussian process, and V is a potential function reflecting the probability density of $\mathscr{F}$. As the system is computationally evolved in time according to Eq. (4), the $\mathbf{f}_j$'s are stochastically propagated on the surface of V, leading to different metastable states that are interpreted as clusters.

The output of the algorithm is a partitioning of patients into separate clusters based on their radiomic expression, such that patients in the same cluster share intrinsic radiomic properties that are different from patients in other clusters. The optimal number of clusters is determined automatically based on a data fidelity constraint set to achieve an equilibrium distribution between the stochastic (i.e., $n(t)$) and deterministic (i.e., $-\nabla \mathrm{V}(\mathbf{f}_j) - \frac{d\mathbf{f}_j}{dt}$) terms of Eq. (4). For more details, including theory, proofs, experimental validation, and benchmark results, we refer the reader to 32. Data clustering was performed in Matlab (MathWorks, Natick, MA).

2.G. Association of clustered radiomic expression patterns with clinical outcome

To test the potential association between the clustered radiomic expression patterns and residual or recurrent disease, the distribution of cancer residual/recurrence events was compared across different patient clusters. Chi-squared tests were used to test for statistical significance, where $P \leq 0.05$ was considered statistically significant. To assess the potential association between the clustered radiomic expression patterns and RFS, independent Kaplan-Meier analyses were performed on different patient clusters. For a given cluster, a Kaplan-Meier estimator was constructed using only RFS data obtained from patients in that cluster. The statistical separation between cluster-derived Kaplan-Meier curves was evaluated using log rank tests, where $P \leq 0.05$ was considered statistically significant. Kaplan-Meier analysis was performed in Matlab (MathWorks, Natick, MA) using the *MatSurv* package.[33]

2.H. Low-dimensional dissection of clustering mechanics

We implemented a *bi-clustering* procedure and unsupervised data reduction technique to identify the principal radiomic features driving the clustering process. Here, the columns of $\mathscr{F}$ (i.e., the set of patients, $\mathbf{f}_j$) and the rows of $\mathscr{F}$ (i.e., the set of features, $\mathbf{f}_i$) were clustered *simultaneously* to generate *column-wise* patient clusters and *row-wise* feature clusters, respectively. For each *row-wise* feature cluster, the top 4 features representing the largest median difference between *column-wise* patient clusters were identified. These features represent a subset of $\mathscr{F}$ that both maximizes the separation of patients into column-clusters and minimizes the redundancy of those clusters by requiring selection across different row-clusters. These radiomic characteristics were investigated to generate low-dimensional, qualitative conclusions about the otherwise high-dimensional signal.

2.I. Radiomic expression adjusted for conventional prognostic clinical features

To test whether radiomic expression provides prognostic value beyond conventional features commonly used for clinical management of head and neck cancer, Cox proportional hazards analysis was used to adjust radiomics for T stage, N stage, HPV status, and change in tumor volume after 20 Gy. Additionally, because some radiomic features are known to demonstrate strong volume effects, we performed a Spearman correlation analysis between the extracted features and tumor volume. Due to the *large m, small n* nature of the problem, individual radiomic features were *not* used as covariates, but instead radiomic cluster (e.g., 1, 2, 3, etc.) was considered an aggregate, low-dimensional measure of radiomic expression and was treated as a Cox covariate.

T and N staging was scored according to the American Joint Committee on Cancer (AJCC) 7th Edition criteria. Change in tumor volume was calculated as the difference in GTVp on intra-treatment CT imaging relative to pre-treatment CT imaging. HPV status was considered as a covariate because HPV-related and HPV-negative OPC tumors are known to exhibit different biologic behaviors as demonstrated by their disparate prognoses. In total, three Cox models were studied: (1) a univariate radiomics-only model,

where *Radiomic Cluster* was interpreted as the covariate; (2) univariate models based on the four clinical features (i.e., *T Stage*, *N Stage*, *HPV-Status*, and *Change in Tumor Volume*); and (3) a multivariate model based on both radiomics and clinical features. The log-likelihood, ℓ, ratio statistic was computed to compare the radiomics only model relative to the radiomics model adjusted for the clinical features. Cox analysis was performed in Matlab using the *Coxphfit* function ($p \leq 0.05$ was considered statistically significant).

3. RESULTS

3.A. Patient characteristics

Between February 2012 and May 2016, 110 head and neck cancer patients were enrolled on the trial, including 82 patients with OPC. Eight OPC patients withdrew from the study prior to receiving intra-treatment ^{18}F-FDG-PET/CT, 1 died of cardiac arrest during treatment, and 1 was lost to follow-up after completing treatment. Among the remaining 72 OPC patients who completed therapy, 8 patients were excluded due to: diagnosis with p16-positive head and neck squamous cell carcinoma of unknown primary (n = 4); prior surgical resection of primary tumor (n = 2); presence of multiple synchronous primary tumors (n = 1); and receipt of neoadjuvant chemotherapy prior to definitive radiotherapy (n = 1). This left 64 patients who qualified for radiomic analysis. The median patient age at the time of treatment initiation was 59.2 ± 9.0 years. Patients were predominantly male (n = 53). Regarding HPV status, 89% (n = 57) were HPV-positive or p16-positive. Initial complete clinical response was achieved in 92.2% (n = 59) of patients. On long-term clinical follow-up, 21.9% (n = 14) of patients demonstrated residual or recurrent disease. The median follow-up time was 3.9 years.

3.B. Intrinsic prognostic value of intra-treatment radiomic expression

Different clustering solutions – driven by underlying changes in radiomic expression pattern due to treatment – were detected after 2 weeks of therapy (Fig. 2), relative to baseline (Fig. 3). We identified a statistically significant association between three intra-treatment clusters and the presence of either residual disease or subsequent recurrence ($P = 0.0256$, χ^2 test). Furthermore, RFS differed for patients in these clusters with a hazard ratio (HR) of 10.54 for the high-risk group compared to the low-risk group ($P = 0.0053$, log-rank test, 95% CI = 2.56–43.38).

Mathematically, Cluster 1 and Cluster 2 were represented by nearly non-degenerate local minima of the optimization function (V, Eq. 4) reflecting the probability density of the

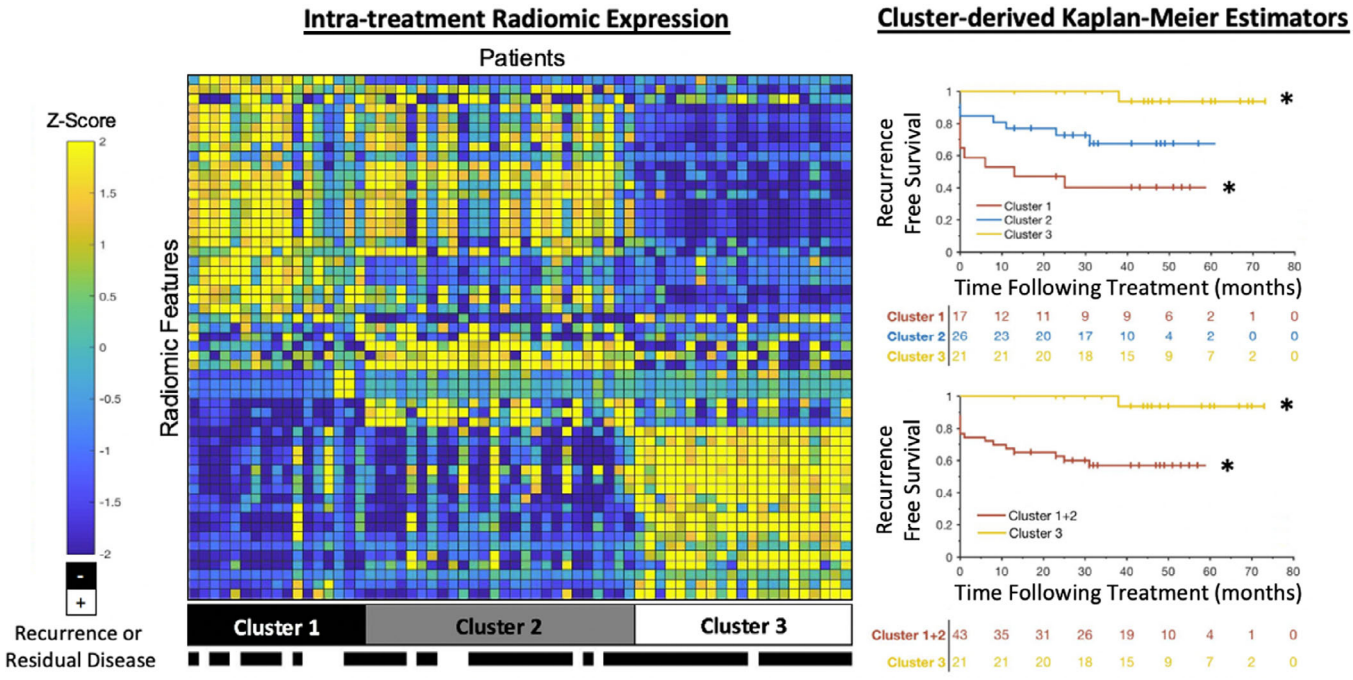

FIG. 2. Unsupervised clustering of intra-treatment radiomic expression with corresponding disease status and cluster-derived Kaplan-Meier estimators of recurrence free survival. The heatmap represents the bi-clustered radiomic feature-space extracted from the primary tumor volume on intra-treatment ^{18}F-FDG-PET imaging. Column vectors denote patient-specific radiomic signatures measured after 20 Gy of initial therapy. Unsupervised clustering resulted in three groups of patients sharing intrinsic similarities in radiomic expression. Disease status is indicated below the heatmap (black, no evidence of residual or recurrent disease during follow-up; white, residual disease at completion of radiation therapy and/or subsequent disease recurrence). Residual/recurrent disease was associated with the three intra-treatment radiomic clusters ($p = 0.0256$, χ^2 test). Kaplan-Meier estimators of recurrence free survival, which were naïvely derived from the clustering partitions, demonstrate prognostic value of intra-treatment radiomic expression. Asterisks denote pair-wise statistical significance between two survival curves. [Color figure can be viewed at wileyonlinelibrary.com]

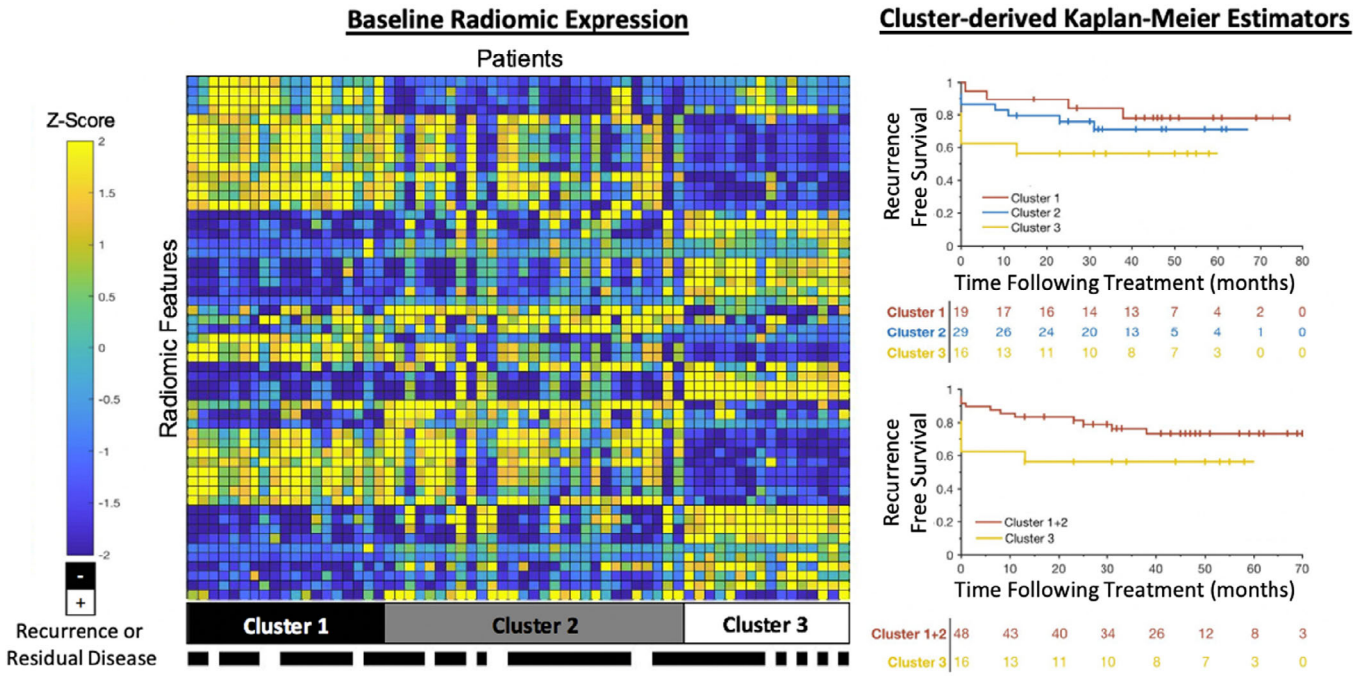

FIG. 3. Unsupervised clustering of baseline radiomic expression with corresponding disease status and cluster-derived Kaplan-Meier estimators of recurrence free survival. The heatmap represents the bi-clustered radiomic feature-space extracted from the primary tumor volume on pre-treatment ^{18}F-FDG-PET imaging. Column vectors denote patient-specific baseline radiomic signatures measured before therapy. Unsupervised clustering resulted in three groups of patients sharing intrinsic similarities in radiomic expression. Disease status is indicated below the heatmap (black, no evidence of residual or recurrent disease during follow-up; white, residual disease at completion of radiation therapy and/or subsequent disease recurrence). Residual/recurrent disease was not associated with the three pre-treatment radiomic clusters ($P = 0.9405$, χ^2 test). Kaplan-Meier estimators of recurrence free survival, which were naïvely derived from the clustering partitions, demonstrate a lack of prognostic value of pre-treatment radiomic expression. [Color figure can be viewed at wileyonlinelibrary.com]

radiomic space.[32] Conceptually, this implies that a larger, more general group of patients with similar radiomic expression were defined by the combination of Cluster 1 and Cluster 2. Kaplan-Meier analysis confirmed that this combined cluster (i.e., Cluster 1 + Cluster 2 on Fig. 2) had significantly shorter RFS relative to Cluster 3 (HR = 7.53, 95% CI = 2.54–22.3; $P = 0.0201$, log-rank test). Thus, this simplified bi-partitioning of patients based on intra-treatment radiomic expression was found to encode prognostic value.

In contrast, pre-treatment radiomic expression was not associated with clinical outcome (Fig. 3). Unsupervised clustering applied independently to the pre-treatment radiomics data resulted in different patients grouped together with nominal separation in RFS: HR = 0.93 for Cluster 1 vs. Cluster 2 (95% CI = 0.27–3.29; $P = 0.9162$, log-rank test), HR = 0.73 for Cluster 1 vs. Cluster 3 (95% CI = 0.18–2.97; $P = 0.6521$, log-rank test), and HR = 0.79 for Cluster 2 vs. Cluster 3 (95% CI = 0.21–2.10; $P = 0.7076$, log-rank test). These results collectively indicate that radiomic expression after 20 Gy, but not at baseline, may indicate early response to radiotherapy for OPC.

3.C. Low-dimensional dissection of intra-treatment radiomic clustering mechanics

As summarized in Fig. 4a, intra-treatment clustering results were primarily influenced by several key radiomic features. Here, the resulting row-wise feature-clusters (denoted as A and B to differentiate them from their orthogonal column-wise patient-cluster counterparts) represent the defining characteristics that influenced radiomic signal divergence after 2 weeks of therapy. Both Cluster 1 and Cluster 2 were enriched with features designed to capture fine image heterogeneities, overall image brightness, and high image intensity (e.g., Cluster Tendency,[34] Dissimilarity,[34] Sum Average,[34] and Short Run High Gray Emphasis[35]). This implies that metabolic heterogeneity and high ^{18}F-FDG uptake after 2 weeks of therapy was generally associated with a poor prognosis. In contrast, Cluster 3 was enriched with features designed to capture coarse image homogeneities and low image intensity (e.g., Low Gray Run Emphasis,[32] Long Run Low Gray Emphasis,[35] Large Zone Emphasis,[36] and Large Size Low Gray Emphasis[36]). This implies that metabolic homogeneity and low ^{18}F-FDG uptake after 2 weeks of therapy was generally associated with a favorable prognosis.

These results demonstrate the magnitude of ^{18}F-FDG uptake, as well as the metabolic spatial heterogeneity of the disease, correlate with treatment response to 20 Gy. A representative case in Fig. 4b demonstrates this phenomenon by comparing two images taken from Cluster 1 and Cluster 3. Differences in metabolic heterogeneity are visually appreciable for images with a comparable maximum standard uptake value (SUV_{max}), which is a radiomic feature on PET that does not encode spatial information. This demonstrates the

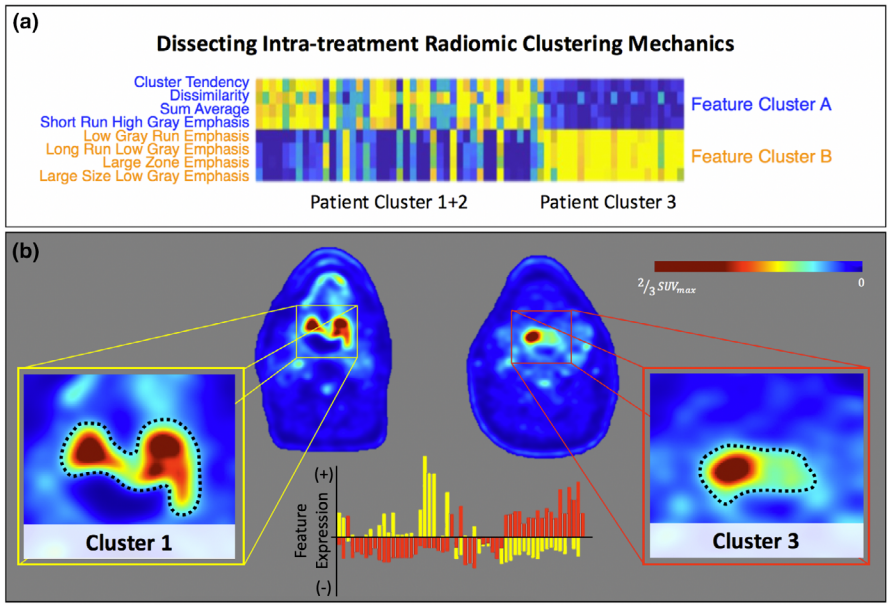

FIG. 4. Dissecting intra-treatment radiomic clustering mechanics. (a) Bi-clustering results demonstrating the most influential features responsible for cluster formation. Each column vector represents a reduced (8-dimensional) patient-specific radiomic signature, whose feature basis is the dominating effect driving cluster formation. This sub-set of features provided the largest separation between patient clusters. Clusters 1 & 2 were collectively associated with poor prognosis and were enriched with features capturing metabolic heterogeneity and high ^{18}F-FDG uptake. Cluster 3 was associated with favorable prognosis and was enriched with metabolic homogeneity and low ^{18}F-FDG uptake. (b) An illustrating example of two patient images from Clusters 1 and 3. Differences in metabolic heterogeneity are visually appreciated for two base of tongue tumors that share a comparable maximum standard uptake value (SUV_{max}), demonstrating the importance of image texture to predicting treatment response. The color-coded bar graph demonstrates the relative difference in quantitative radiomic expression associated with each tumor (yellow, tumor from Cluster 1; red, tumor from Cluster 3). [Color figure can be viewed at wileyonlinelibrary.com]

importance of extending quantitative analyses beyond SUV_{max} measurements and incorporating more complex features such as image texture to develop computational biomarkers that better correlate with outcome.

3.D. Radiomic expression adjusted for conventional prognostic clinical features

Cox proportional hazards modeling results are summarized in Tables I–IV, where radiomic expression is compared to clinical features commonly used for management and prognostication of head and neck cancer. Table I shows univariate Cox analysis with *Radiomic Cluster* as a covariate, which was significant for RFS (unadjusted HR = 2.70; 95% CI = 1.26–5.76; $P = 0.01$; $\ell = -49.6329$). Table II shows the univariate Cox model for each clinical feature, of which *Change in Tumor Volume* and *HPV-Status* were both significant for RFS on univariate analysis (HR = 1.08; 95% CI =-1.01–1.17; $P = 0.03$ and HR = 0.25; 95% CI = 0.06–1.04; $P = 0.05$, respectively).

Multivariate Cox modeling results are summarized in Tables III and IV. As demonstrated in Table III, *Radiomic Cluster* maintained significance with RFS when adjusted for T and N tumor staging, HPV status, and change in primary tumor volume (adjusted HR = 2.69; 95% CI = 1.03–7.04; $P = 0.04$; $\ell = -52.3653$). Based on log-likelihood ratios, *Change in Tumor Volume*, *HPV-Status*, and *Tumor Stage* were not statistically significant variables given the variable *Radiomic Cluster* in the extended multivariate Cox model. For completion, Table IV summarizes multivariate Cox analysis based on *only* clinical features, which was not significant for RFS.

The average pre-treatment and intra-treatment tumor volume was 18.9 ± 18.1 cm^3 (range, 1–90.8 cm^3) and

TABLE I. Univariate Cox proportional hazards model of recurrence free survival based on radiomic cluster as a covariate.

Univariate Cox Proportional Hazards Model (Radiomic Cluster)		
Variable	Unadjusted HR (95% CI)	*P* value
Radiomic Cluster	2.70 (1.26-5.76)	0.01

Abbreviations: CI = confidence interval; HR = Hazard Ratio.

TABLE II. Univariate Cox proportional hazards model of recurrence free survival based on clinical features of head and neck cancer: T and N tumor staging, HPV status, and change in tumor volume after 20 Gy.

Univariate Cox Proportional Hazards Models (Clinical Features of Head and Neck Cancer)		
Variable	Adjusted HR (95% CI)	*P* value
T Stage	1.56 (0.94-2.58)	0.08
N Stage	1.08 (0.68-1.73)	0.74
Change in Tumor Volume	1.08 (1.01-1.17)	0.03
HPV Status	0.25 (0.06-1.04)	0.05

Abbreviations: CI, confidence interval; HR, Hazard Ratio.

TABLE III. Multivariate Cox proportional hazards model of recurrence free survival based on radiomic cluster adjusted for conventional disease staging, HPV status, and change in tumor volume after 20 Gy.

Multivariate Cox Proportional Hazards Model (Radiomics Adjusted for Clinical Features of Head and Neck Cancer)		
Variable	Adjusted HR (95% CI)	*P* value
Radiomic Cluster	2.69 (1.03-7.04)	0.04
T Stage	1.06 (0.54-2.07)	0.85
N Stage	1.26 (0.72-2.20)	0.42
Change in Tumor Volume	1.05 (0.99-1.12)	0.09
HPV Status	0.55 (0.12-2.57)	0.44

Abbreviations: CI, confidence interval; HR, Hazard Ratio.

TABLE IV. Multivariate Cox proportional hazards model of recurrence free survival based on clinical features of head and neck cancer: T and N tumor staging, HPV status, and change in tumor volume after 20 Gy.

Multivariate Cox Proportional Hazards Model (Clinical Features of Head and Neck Cancer without Radiomics)		
Variable	Adjusted HR (95% CI)	*P* value
T Stage	1.56 (0.91-2.69)	0.10
N Stage	1.13 (0.68-1.87)	0.64
Change in Tumor Volume	1.06 (0.99-1.13)	0.08
HPV Status	0.53 (0.10-2.91)	0.46

Abbreviations: CI, confidence interval; HR, Hazard Ratio.

11.7 ± 15.2 cm^3 (range, 0.5–67.9 cm^3), respectively. Twelve radiomic features were correlated with intra-treatment tumor volume and 2 features were correlated with change in tumor volume (Table S3). None of these volume-associated radiomic features were major drivers of cluster formation as reported in Fig. 4 and their exclusion did not affect clustering results. This implies that FDG texture provides complementary information to CT volumetry.

Collectively, these results demonstrate that intra-treatment radiomic expression may provide complementary value above and beyond what can be currently obtained with prognostic indications commonly used for clinical management and prognostication of head and neck cancer.

4. DISCUSSION

Phenotypic changes on cancer images are a hallmark of treatment response assessment. Radiomic expression – which may be linked to the appearance and behavior of disease – may encode traces of therapeutic response that can be computationally measured in individual patients. This research developed an unsupervised machine learning approach to quantify early metabolic response based on intrinsic radiomic expression patterns on ^{18}F-FDG-PET images during radiation therapy. Our decision to investigate PET radiomics in this particular study was motivated by current clinical trial design at our institution and others, where treatment de-intensification is being considered based on changes in HPV-positive tumor metabolism.[8,37] We note, however, that the extension of our approach to incorporate CT radiomics may potentially lead to improved findings, which in turn may motivate new clinical trial design based on multi-modal radiomic analysis.

In our study, a significant difference in cluster formation was observed between pre-treatment and intra-treatment imaging, indicating that the underlying radiomic signal changed after 2 weeks and 20 Gy. While the pre-treatment radiomic signature did not correlate with treatment outcome, intra-treatment radiomic expression was significantly associated with both residual/recurrent disease status and RFS. This finding suggests that intra-treatment ^{18}F-FDG-PET radiomic expression may represent a noninvasive biomarker of early treatment response in patients with OPC, regardless of baseline metabolic imaging characteristics.

The formation of intra-treatment clusters was heavily influenced by several key radiomic characteristics. In particular, clusters associated with poor prognosis were characterized by imaging features that represent aspects of spatial heterogeneity at high intensity. In contrast, clusters associated with favorable prognosis exemplified homogeneous, low intensity image information. For example, the feature *short run high gray emphasis* (SRHGE) is a measure of both image intensity and coarse heterogeneity.[35] In general, this feature quantifies the joint-distribution between the magnitude of ^{18}F-FDG uptake and its spatial dependence throughout the tumor. On PET, high SRHGE values indicate metabolically active, heterogeneous disease. In our data, SRHGE was expressed in clusters linked to poor outcome. This indicates that patients presenting with metabolically active, heterogeneous primary tumors after 2 weeks of radiation therapy typically resulted in a worse prognosis. In contrast, the feature *large zone emphasis* (LZE) was commonly expressed in patients with favorable outcome. LZE is a texture feature of coarse image homogeneity[36]; on PET high values indicate uniform ^{18}F-FDG uptake throughout the tumor regardless of intensity magnitude. This finding implies that patients with metabolically homogeneous disease after 2 weeks of radiation therapy typically presented with a better prognosis.

Our data therefore provide evidence that metabolic spatial heterogeneity – in addition to the magnitude of ^{18}F-FDG uptake – is associated with long term treatment outcome. From a biological perspective, metabolic heterogeneity and increased overall ^{18}F-FDG uptake may potentially be a surrogate for hypoxia.[38] We hypothesize that necrotic tumor regions consume less glucose, resulting in a spatial heterogeneity of the PET signal. This hypothesis is consistent with the theoretical framework for glycolysis proposed by Alfarouk et al.,[39] as well as experimental data demonstrating that preclinical tumor models of head and neck cancer exhibit increased intratumoral metabolic heterogeneity.[40] Evidence also suggests that heterogeneous ^{18}F-FDG texture may be associated with hypoxia radiotracers such as ^{18}F-fluoromisonidazole.[30,41–46] We note that because texture analysis is particularly sensitive to image gray level discretization,[30,47–50] caution is advised when calculating

radiomic texture features. In fact, it has been suggested that not all radiomic features should be calculated at the same discretized dynamic range and that texture optimization may have a significant influence on prognostic potential.[51]

Since we did not observe any prognostic value in baseline metabolism, our data suggests that early response is potentially a threshold mechanism that depends on whether or not hypoxia is resolved after initial treatment. While this conclusion remains limited and warrants further investigation, the lack of prognostic value that we observed on pre-treatment imaging is consistent with a recent paper published by Ger et al.[52] In their study, they found that baseline PET/CT radiomic features were not associated with clinical outcomes in the largest cohort of head and neck cancer patients to date. However, several other studies have in fact demonstrated associations between pre-treatment radiomics and outcomes across a variety of head and neck cancer sites.[14–17,19,20] Several key differences in methodology may contribute to different conclusions.

While most published radiomic studies rely on retrospective data, our results are based on a prospective clinical trial where all images were acquired on the same scanner under the same acquisition protocol. It is generally well-known that radiomic features are susceptible to scanner variation and inter-observer variability,[53] which can often lead to inconsistent downstream machine learning models.[54,55] To the best of our knowledge, our study is the first reported head and neck cancer radiomic analysis based on prospectively acquired intra-treatment ^{18}F-FDG-PET images and long-term clinical follow-up. Our findings are therefore strengthened by a high-fidelity dataset representing a homogenous patient cohort without inter-scanner variability across different vendors, models, or acquisition protocols.

Furthermore, while previous studies have typically utilized *supervised* machine learning models, we focused instead on *unsupervised* machine learning. Unlike supervised techniques – which rely on a training dataset to map the relationship between features and depend variables based on explicit observation – unsupervised learning instead investigates the intrinsic properties of data with fewer assumptions. Such approaches have demonstrated meaningful non-parametric associations between radiomics data and various clinical and/or biological endpoints.[13,56,57]

When adjusted for conventional prognostic factors, including T and N staging, changes in tumor volume, and HPV status, the relationship between RFS and intra-treatment radiomic expression was preserved. This is an important conclusion because studies have reported that radiomic texture features are sometimes biased by tumor volume.[58–60] Furthermore, this finding also suggests that radiomic expression after 20 Gy may provide complementary prognostic value for patients with HPV-related disease. This may have potential for high clinical impact, as approximately 20% of patients with HPV-positive OPC still experience disease recurrence within 5 years following treatment.[61] Identification of patients with HPV-related disease and poor prognosis is essential in light of ongoing efforts to safely de-escalate therapy for this patient population with generally favorable treatment outcomes.[6–8] Radiomics may facilitate a finer stratification of HPV-positive OPC patients into candidate risk groups for novel adaptive therapy regimens. For example, patients with radiomic signatures indicative of favorable early response may be candidates for therapeutic de-escalation protocols that reduce acute and long-term toxicity profiles. Similarly, high-risk patients may benefit from therapeutic intensification and closer follow-up, potentially including monitoring HPV circulating tumor DNA[62] and similar radiogenomic analyses of liquid biopsies.[63,64]

This paper presents a novel approach to quantifying early metabolic response of OPC, but it has several limitations. First, we chose to study radiomic expression of the primary disease site and excluded imaging features of the nodal disease. This is a limitation because lymph node status is an important staging/prognostic parameter for patients with head and neck cancer. While prior radiomic studies have historically focused on the primary disease site due to technical limitations, a recent study did demonstrate the prognostic value of radiomic features derived from the lymph nodes.[65] Nevertheless, our results demonstrate that radiomic expression of the primary tumor is prognostic, even when adjusted for T and N stage, HPV status, and tumor volume. This implies that intra-treatment radiomic expression provides added value above and beyond what can be obtained with conventional disease stage prognostication.

A second limitation of this study is that it did not account for either intra- or inter-observer variability in tumor segmentation. This represents a clear challenge in radiomics, as some features may be highly sensitive to segmentation differences.[47,48] Reproducibility of results should therefore be studied in future work, either through observer studies or using deep learning segmentation algorithms that may reduce variability.[66]

Finally, the most important limitation of this study is the absence of an independent dataset with which to evaluate the generalization of our results. Since our analysis is based on an investigational imaging protocol within the context of a prospective clinical trial, external evaluation is non-trivial at this time. To compensate for this limitation methodologically, we strategically chose an unsupervised clustering formalism that is less prone to hyper-parameter tuning and over-fitting compared to supervised learning, which would likely be overfit given our limited sample size. Nevertheless, the lack of external testing represents a significant limitation to the conclusions drawn from this study.

5. CONCLUSIONS

This study demonstrated the prognostic value and clinical utility of intra-treatment metabolic image interrogation, which may guide adaptive therapy strategies for OPC and serve as a blueprint for other disease sites. The quality of our study is strengthened by its prospective image acquisition protocol, homogenous patient cohort, relatively long patient follow-up times, and unsupervised clustering formalism that

is less prone to hyper-parameter tuning and over-fitting compared to supervised learning. Our results suggest that intra-treatment ^{18}F-FDG-PET radiomic expression serves as an early marker of radiation resistance and is intrinsically associated with both recurrence/residual disease and RFS. The particular radiomic characteristics that correlate with clinical outcomes suggest that metabolic spatial heterogeneity after 20 Gy portends complete and durable therapeutic response. This finding was independent of baseline metabolic imaging characteristics and conventional clinical prognostic factors, thus providing an advantage over existing approaches.

CONFLICT OF INTERESTS

The authors report no conflicts of interest.

DATA AVAILABILITY STATEMENT

Research data are stored in an institutional repository and deidentified data will be shared upon request to the corresponding author through a data use agreement.

[a]Author to whom correspondence should be addressed. Electronic mail: kyle.lafata@duke.edu; Telephone: (978) 491-8730.

REFERENCES

1. Ang KK, Harris J, Wheeler R, et al. Human papillomavirus and survival of patients with oropharyngeal cancer. *N Engl J Med*. 2010;363:24–35.
2. Huang SH, Xu W, Waldron J, et al. Refining American Joint Committee on Cancer/Union for International Cancer Control TNM stage and prognostic groups for human papillomavirus-related oropharyngeal carcinomas. *J Clin Oncol*. 2015;33:836–845.
3. O'Sullivan B, Huang SH, Su J, et al. Development and validation of a staging system for HPV-related oropharyngeal cancer by the International Collaboration on Oropharyngeal cancer Network for Staging (ICON-S): A multicentre cohort study. *Lancet Oncol*. 2016;17:440–451.
4. Worden FP, Kumar B, Lee JS, et al. Chemoselection as a strategy for organ preservation in advanced oropharynx cancer: Response and survival positively associated With HPV16 copy number. *J Clin Oncol*. 2008;26:3138–3146.
5. Chaturvedi AK, Engels EA, Pfeiffer RM, et al. Human papillomavirus and rising oropharyngeal cancer incidence in the United States. *J Clin Oncol*. 2011;29:4294–4301.
6. Adelstein DJ, Ismaila N, Ku JA, et al. Role of treatment deintensification in the management of p16+ oropharyngeal cancer: ASCO provisional clinical opinion. *J Clin Oncol*. 2019;37:1578–1589.
7. Heukelom J, Fuller CD. Head and neck cancer adaptive radiation therapy (ART): Conceptual considerations for the informed clinician. *Semin Radiat Oncol*. 2019;29:258–273.
8. Mowery YM, Vergalasova I, Rushing CN, et al. Early ^{18}F-FDG-PET response during radiation therapy for HPV-related oropharyngeal cancer may predict disease recurrence. *Int J Radiat Oncol Biol Phys*. 2020: S0360-3016:34118–34123.
9. Ferris RL, Blumenschein G, Fayette J, et al. Nivolumab for recurrent squamous-cell carcinoma of the head and neck. *N Engl J Med*. 2016;375:1856–1867.
10. Burtness B, Harrington KJ, Greil R, et al. KEYNOTE-048 Investigators. Pembrolizumab alone or with chemotherapy versus cetuximab with chemotherapy for recurrent or metastatic squamous cell carcinoma of the head and neck (KEYNOTE-048): A randomised, open-label, phase 3 study. *Lancet*. 2019;394:1915-1928.
11. Mehanna H, Robinson M, Hartley A, et al. De-ESCALaTE HPV Trial Group. Radiotherapy plus cisplatin or cetuximab in low-risk human papillomavirus-positive oropharyngeal cancer (De-ESCALaTE HPV): An open-label randomised controlled phase 3 trial. *The Lancet*. 2019;393:51–60.
12. Gillison ML, Trotti AM, Harris J, et al. Radiotherapy plus cetuximab or cisplatin in human papillomavirus-positive oropharyngeal cancer (NRG Oncology RTOG 1016): A randomised, multicentre, non-inferiority trial. *The Lancet*. 2019;393:40–50.
13. Aerts H, Velazquez E, Leijenaar R, et al. Decoding tumour phenotype by noninvasive imaging using a quantitative radiomics approach. *Nat Commun*. 2014;5:4006.
14. Folkert MR, Setton J, Apte AP, et al. Predictive modeling of outcomes following definitive chemoradiotherapy for oropharyngeal cancer based on FDG-PET image characteristics. *Phys Med Biol*. 2017;62:5327–5343.
15. Vallières M, Kay-Rivest E, Perrin LJ, et al. Radiomics strategies for risk assessment of tumour failure in head-and-neck cancer. *Sci Rep*. 2017;7:10117.
16. Bogowicz M, Leijenaar RTH, Tanadini-Lang S, et al. Post-radiochemotherapy PET radiomics in head and neck cancer - The influence of radiomics implementation on the reproducibility of local control tumor models. *Radiother Oncol*. 2017;125:385–391.
17. M. D. Anderson Cancer Center Head and Neck Quantitative Imaging Working Group. Investigation of radiomic signatures for local recurrence using primary tumor texture analysis in oropharyngeal head and neck cancer patients. *Sci Rep*. 2018;8:1524.
18. Bogowicz M, Riesterer O, Stark LS, et al. Comparison of PET and CT radiomics for prediction of local tumor control in head and neck squamous cell carcinoma. *Acta Oncol*. 2017;56:1531–1536.
19. Parmar C, Grossmann P, Rietveld D, Rietbergen MM, Lambin P, Aerts HJ. Radiomic machine-learning classifiers for prognostic biomarkers of head and neck cancer. *Front Oncol*. 2015;3:272.
20. Ou D, Blanchard P, Rosellini S, et al. Predictive and prognostic value of CT based radiomics signature in locally advanced head and neck cancers patients treated with concurrent chemoradiotherapy or bioradiotherapy and its added value to Human Papillomavirus status. *Oral Oncol*. 2017;71:150–155.
21. Zhang B, He X, Ouyang F, et al. Radiomic machine-learning classifiers for prognostic biomarkers of advanced nasopharyngeal carcinoma. *Cancer Lett*. 2017;10:21–27.
22. Pota M, Scalco E, Sanguineti G, et al. Early prediction of radiotherapy-induced parotid shrinkage and toxicity based on CT radiomics and fuzzy classification. *Artif Intell Med*. 2017;81:41–53.
23. van Dijk LV, Noordzij W, Brouwer CL, et al. ^{18}F-FDG PET image biomarkers improve prediction of late radiation-induced xerostomia. *Radiother Oncol*. 2018;126:89–95.
24. Thor M, Tyagi N, Hatzoglou V, et al. A magnetic resonance imaging-based approach to quantify radiation-induced normal tissue injuries applied to trismus in head and neck cancer. *Phys Imaging Radiat Oncol*. 2017;1:34–40.
25. Abdollahi H, Mostafaei S, Cheraghi S, Shiri I, Rabi Mahdavi S, Kazemnejad A. Cochlea CT radiomics predicts chemoradiotherapy induced sensorineural hearing loss in head and neck cancer patients: A machine learning and multi-variable modelling study. *Phys Med*. 2018;45:192–197.
26. van Dijk LV, Thor M, Steenbakkers RJHM, et al. Parotid gland fat related Magnetic Resonance image biomarkers improve prediction of late radiation-induced xerostomia. *Radiother Oncol*. 2018;128:459–466.
27. Gabryś HS, Buettner F, Sterzing F, Hauswald H, Bangert M. Design and selection of machine learning methods using radiomics and dosiomics for normal tissue complication probability modeling of xerostomia. *Front Oncol*. 2018;5:35.
28. Zwanenburg A, Leger S, Vallieres M, Lock S. Image biomarker standardisation initiative reference manual. arXiv preprint arXiv: 1612.07003.
29. Zwanenburg A, Vallières M, Abdalah MA, et al. The image biomarker standardization initiative: Standardized quantitative radiomics for high-throughput image-based phenotyping. *Radiology*. 2020;295:328–338.
30. Orlhac F, Soussan M, Maisonobe JA, Garcia CA, Vanderlinden B, Buvat I. Tumor texture analysis in 18F-FDG PET: Relationships between texture parameters, histogram indices, standardized uptake values,

metabolic volumes, and total lesion glycolysis. *J Nucl Med*. 2014;55 (3):414–422.
31. Chang Y, Lafata K, Wang C, et al. Digital phantoms for characterizing inconsistencies among radiomics extraction toolboxes. *Biomed Phys Eng Express*. 2020;6:025016.
32. Lafata K, Zhou Z, Liu J, Yin FF. Data clustering based on Langevin annealing with a self-consistent potential. *Q Appl Math*. 2018;77 (3):591–613. http://dx.doi.org/10.1090/qam/1521
33. Creed J, Gerke T, Berglund A. MatSurv: Survival analysis and visualization in MATLAB. *J Open Source Software*. 2020;5:1830.
34. Haralick RM, Shanmugam K, Dinstein I. Textural features for image classification. *IEEE Trans Systems Man Cybernetics*. 1973;SMC-3 (6):610–621.
35. Tang X. Texture information in run-length matrices. *IEEE Trans Image Process*. 1998;7:1602–1609.
36. Thibault G, Fertil B, Navarro C, et al. Texture indexes and gray level size zone matrix. Application to cell nuclei classification. *Pat Rec Inf Proc*. 2009;140–145.
37. Pollom EL, Song J, Durkee BY, et al. Prognostic value of midtreatment FDG-PET in oropharyngeal cancer. *Head Neck*. 2016;38:1472–1478.
38. Brizel DM, Sibley GS, Prosnitz LR, Scher RL, Dewhirst MW. Tumor hypoxia adversely affects the prognosis of carcinoma of the head and neck. *Int J Radiat Oncol Biol Phys*. 1997;38:285–289.
39. Alfarouk KO, Verduzco D, Rauch C, et al. Glycolysis, tumor metabolism, cancer growth and dissemination. A new pH-based etiopathogenic perspective and therapeutic approach to an old cancer question. *Oncoscience*. 2014;1:777–802.
40. Nakajima EC, Laymon C, Oborski M, et al. Quantifying metabolic heterogeneity in head and neck tumors in real time: 2-DG uptake is highest in hypoxic tumor regions. *PLoS One*. 2014;9:e102452.
41. Yamada T, Uchida M, Kwang-Lee K, et al. Correlation of metabolism/hypoxia markers and fluorodeoxyglucose uptake in oral squamous cell carcinomas. *Oral Surg Oral Med Oral Pathol Oral Radiol*. 2012;113:464–471.
42. Rajendran JG, Schwartz DL, O'Sullivan J, et al. Tumor hypoxia imaging with [F-18] Fluoromisonidazole positron emission tomography in head and neck cancer. *Clin Cancer Res*. 2006;12:5435–5441.
43. Kikuchi M, Yamane T, Shinohara S, et al. 18F-fluoromisonidazole positron emission tomography before treatment is a predictor of radiotherapy outcome and survival prognosis in patients with head and neck squamous cell carcinoma. *Ann Nucl Med*. 2011;25:625–633.
44. Zips D, Zöphel K, Abolmaali N, et al. Exploratory prospective trial of hypoxia-specific PET imaging during radiochemotherapy in patients with locally advanced head-and-neck cancer. *Radiother Oncol*. 2012;105:21–28.
45. Thorwarth D, Eschmann SM, Holzner F, Paulsen F, Alber M. Combined uptake of [18F]FDG and [18F]FMISO correlates with radiation therapy outcome in head-and-neck cancer patients. *Radiother Oncol*. 2006;80:151–156.
46. Kroenke M, Hirata K, Gafita A, et al. Voxel based comparison and texture analysis of ^{18}F-FDG and ^{18}F-FMISO PET of patients with head-and-neck cancer. *PLoS One*. 2019;14:e0213111.
47. Altazi BA, Zhang GG, Fernandez DC, et al. Reproducibility of F18-FDG PET radiomic features for different cervical tumor segmentation methods, gray-level discretization, and reconstruction algorithms. *J Appl Clin Med Phys*. 2017;18:32–48.
48. Lu L, Lv W, Jiang J, et al. Robustness of radiomic features in [^{11}C]Choline and [^{18}F]FDG PET/CT imaging of nasopharyngeal carcinoma: Impact of segmentation and discretization. *Mol Imaging Biol*. 2016;18:935–945.
49. Hatt M, Majdoub M, Vallières M, et al. 18F-FDG PET uptake characterization through texture analysis: Investigating the complementary nature of heterogeneity and functional tumor volume in a multi-cancer site patient cohort. *J Nucl Med*. 2015;56:38–44.
50. Leijenaar RT, Nalbantov G, Carvalho S, et al. The effect of SUV discretization in quantitative FDG-PET Radiomics: The need for standardized methodology in tumor texture analysis. *Sci Rep*. 2015;5:11075.
51. Vallières M, Freeman CR, Skamene SR, El Naqa I. A radiomics model from joint FDG-PET and MRI texture features for the prediction of lung metastases in soft-tissue sarcomas of the extremities. *Phys Med Biol*. 2015;60:5471–5496.
52. Ger RB, Zhou S, Elgohari B, et al. Radiomics features of the primary tumor fail to improve prediction of overall survival in large cohorts of CT- and PET-imaged head and neck cancer patients. *PLoS One*. 2019;14:e0222509.
53. Leijenaar RTH, Carvalho S, Velazquez ER, et al. Stability of FDG-PET Radiomics features: An integrated analysis of test-retest and inter-observer variability. *Acta Oncol*. 2013;52:1391–1397.
54. Lafata K, Cai J, Wang C, Hong J, Kelsey CR, Yin FF. Spatial-temporal variability of radiomic features and its effect on the classification of lung cancer histology. *Phys Med Biol*. 2018;63 (22):225003. http://dx.doi.org/10.1088/1361-6560/aae56a
55. Chang Y, Lafata K, Sun W, et al. An investigation of machine learning methods in delta-radiomics feature analysis. *PLoS One*. 2019;14: e0226348.
56. Lafata KJ, Zhou Z, Liu JG, Hong J, Kelsey CR, Yin FF. An exploratory radiomics approach to quantifying pulmonary function in CT images. *Sci Rep*. 2019;9(1). http://dx.doi.org/10.1038/s41598-019-48023-5
57. Lu H, Arshad M, Thornton A, et al. A mathematical-descriptor of tumor-mesoscopic-structure from computed-tomography images annotates prognostic- and molecular-phenotypes of epithelial ovarian cancer. *Nat Commun*. 2019;10:764.
58. Welch ML, McIntosh C, Haibe-Kains B, et al. Vulnerabilities of radiomic signature development: The need for safeguards. *Radiother Oncol*. 2019;130:2–9.
59. Fave X, Zhang L, Yang J, et al. Impact of image preprocessing on the volume dependence and prognostic potential of radiomics features in non-small cell lung cancer. *Trans Canc Res*. 2016;5:349–363.
60. van Velden F, Nissen I, Lammertsma A, Boellaard R. Dependence of various radiomics features on different imaging characteristics. *J Nucl Med*. 2014;55:2071.
61. Fakhry C, Blackford AL, Neuner G, et al. Association of oral human papillomavirus DNA persistence with cancer progression after primary treatment for oral cavity and oropharyngeal squamous cell carcinoma. *JAMA Oncol*. 20195:985–992.
62. Chera BS, Kumar S, Shen C, et al. Plasma circulating tumor HPV DNA for the surveillance of cancer recurrence in HPV-associated oropharyngeal cancer. *J Clin Oncol*. 2020;38:1050–1058.
63. Corradetti M, Torok J, Hatch A, et al. Dynamic changes in circulating tumor DNA during chemoradiation for locally advanced lung cancer. *Adv Radiat Oncol*. 2019;4:748–752.
64. Lafata KJ, Corradetti M, Gao J, et al. Radiogenomic analysis of locally advanced lung cancer based on CT imaging and intra-treatment changes in cell free DNA. *Radiology: Imaging Cancer*. 2021 (In Press).
65. Bogowicz M, Tanadini-Lang S, Guckenberger M, Riesterer O. Combined CT radiomics of primary tumor and metastatic lymph nodes improves prediction of loco-regional control in head and neck cancer. *Sci Rep*. 2019;9:15198.
66. Cardenas CE, McCarroll RE, Court LE, et al. Deep learning algorithm for auto-delineation of high-risk oropharyngeal clinical target volumes with built-in dice similarity coefficient parameter optimization function. *Int J Radiat Oncol Biol Phys*. 2018;101:468–478.

SUPPORTING INFORMATION

Additional supporting information may be found online in the Supporting Information section at the end of the article.

Table S1. IBSI guidelines for reporting on radiomic studies.
Table S2. List of radiomic features considered in this study.
Table S3. Spearman correlation results between radiomics and tumor volume after 20 Gy.